Journal of Solid State Chemistry 184 (2011) 1867–1874

Contents lists available at ScienceDirect

Journal of Solid State Chemistry

journal homepage: www.elsevier.com/locate/jssc

Titania–lanthanum phosphate photoactive and hydrophobic new generation catalyst

Chembolli K. Jyothi, Kanakkanmavudi B. Jaimy, Swapankumar Ghosh, Sasidharan Sankar, V.S. Smitha, K.G.K. Warrier*

National Institute for Interdisciplinary Science & Technology (NIIST), CSIR, Trivandrum 695019, India

ARTICLE INFO

Article history:
Received 25 February 2011
Received in revised form
5 May 2011
Accepted 15 May 2011
Available online 27 May 2011

Keywords:
Sol–gel process
TiO_2
Nanocomposites
Functional applications

ABSTRACT

Titania–lanthanum phosphate nanocomposites with multifunctional properties have been synthesized by aqueous sol–gel method. The precursor sols with varying TiO_2:$LaPO_4$ ratios were applied as thin coating on glass substrates in order to be transparent, hydrophobic, photocatalytically active coatings. The phase compositions of the composite powders were identified by powder X-ray diffraction (XRD) and high-resolution transmission electron microscopy (HR-TEM). The anatase phase of TiO_2 in TiO_2–$LaPO_4$ composite precursors was found to be stable even on annealing at 800 °C. The glass substrates, coated with TL1 (TiO_2–$LaPO_4$ composition with 1 mol% $LaPO_4$) and TL50 (composite precursor containing TiO_2 and $LaPO_4$ with molar ratio 1:1) sols and annealed at 400 °C, produced contact angles of 74° and 92°, respectively, though it is only 62° for pure TiO_2 coating. The glass substrates, coated with TL50 sol, produced surfaces with relatively high roughness and uneven morphology. The TL1 material, annealed at 800 °C, has shown the highest UV photoactivity with an apparent rate constant, $k_{app}=24\times10^{-3}\,min^{-1}$, which is over five times higher than that observed with standard Hombikat UV 100 ($k_{app}=4\times10^{-3}\,min^{-1}$). The photoactivity combined with a moderate contact angle (85.3°) shows that this material has a promise as an efficient self-cleaning precursor.

1. Introduction

Recently, research into self-cleaning surfaces has become of special interest due to the potentially large reductions in both time and cost of cleaning and maintenance of exposed surfaces [1]. Surfaces with high water contact angles are also known to possess a number of useful properties such as, anti-adhesion [2], anti-contamination [3] and self-cleaning [4]. These surface characteristics are desirable for many industrial and biological applications including antibiofouling paints for boats [5], anti-adhesion of snow for antennas and windows [6], self-cleaning windshields for automobiles [7], metal refining, stain resistant textiles and antisoiling architectural coatings [8]. Exposed surface roughness of the coatings on substrates is one of the important factors in addition to structural hydrophobicity during the preparation of hydrophobic surfaces. The control of coating roughness is pivotal in optimizing the counteracting hydrophobicity and transparency [9]. Much effort has been devoted to mimick the self-cleaning property of the lotus leaf although without substantial success [1]. Some self-cleaning products, such as tiles, glass and plastics, coated with TiO_2-based photocatalysts have become commercially available [1]. The advantage of a TiO_2 based self-cleaning surface is that it can decompose organic contaminants or kill bacteria adhered to the surface upon ultraviolet light exposure [1].

Titanium dioxide, also known as titania, in nanosize range is well recognized as a potential catalyst for many photocatalytic reactions due to its relatively low cost and non-toxic nature. Among the three crystalline forms of titania, the anatase phase has relatively higher photocatalytic activity because of its low electron–hole recombination rate. Thermal stability enhancement of anatase phase in the temperature range 400–800 °C is widely investigated [10,11]. Composite catalysts based on ZnO/In_2O_3 heterostructures [12] and basic bismuth(III) nitrate (BBN)/$BiVO_4$ [13] were reported to show higher photocatalytic activity under UV light irradiation. Hydrophobic properties are introduced by synthesizing nano titania composites using hydrophobic polymers [1], hybrids or also by other inorganic nano particulates. Rare earth phosphates are reasonably hydrophobic [14] and were found to possess catalytic properties [15,16]. Lanthanum phosphate also has excellent structural and thermal stability even at high temperatures [17,18]. Lanthanum phosphate sol, prepared by a simple sol–gel method, has been successfully tested for

* Corresponding author. Fax: +91 471 2491712.
E-mail addresses: swapankumar.ghosh2@mail.dcu.ie (S. Ghosh), wwarrierkgk@yahoo.co.in (K.G.K. Warrier).

0022-4596/$ - see front matter © 2011 Elsevier Inc. All rights reserved.
doi:10.1016/j.jssc.2011.05.020

catalysis applications as nanocoatings and particulates [17]. There are many reports on the use of TiO_2 hybrid sol coatings on glass substrates as photocatalytic surfaces. Titania sol based coatings are usually hydrophilic and may facilitate accumulation of contamination on the coated glass surface [1].

To the best of our knowledge, inorganic biocompatible oxides have not been shown to have hydrophobic surface properties. $LaPO_4$ grows into rod shaped crystals on calcination and is known for its high-temperature phase stability in solid state applications [17], and initial experiments indicated that a composite of rod shaped $LaPO_4$ crystals and spherical TiO_2 has shown relatively higher hydrophobicity [14]. However, there is no published literature on the application of TiO_2–$LaPO_4$ nanocomposites utilizing the enhanced hydrophobicity contributed by $LaPO_4$ as well as the photocatalytic properties of TiO_2 in decomposing the organic pollutants. In addition, the particle size distribution has been selected to enhance surface roughness. This study, therefore, presents an attempt to prepare titanium dioxide–lanthanum phosphate nanocomposite through an innovative sol–gel route. The TiO_2–$LaPO_4$ composite powders were characterized by X-ray diffraction (XRD), Fourier Transform Infrared spectroscopy (FTIR) and transmission electron microscopy (TEM), to ascertain the crystal structure and phase composition. The photoactivity was estimated by methylene blue dye decomposition technique. The hydrophobicity of the composite powders and coated surfaces was measured by dynamic water contact angle and sessile drop methods. The data obtained from the activity, hydrophobicity and surface roughness measurements are discussed and correlated.

2. Experimental

2.1. Chemicals

Titanylsulfate (98%) was procured from M/s. Travancore Titanium Products, Trivandrum, India. Ammonium hydroxide solution (25%) and orthophosphoric acid (88%, analytical grade) were procured from s.d. FINE-CHEM Ltd, India. Methylene blue (MB) dye (analytical grade) and HNO_3 were from Qualigens Fine Chemicals, India. Lanthanum nitrate (99.9%) was purchased from M/s. Indian Rare Earths Ltd., India. Hombikat UV 100 is a commercial titanium dioxide and was procured from Sachtleben Chemie, Germany. All the chemicals were used as received without any further purification.

2.2. Synthesis of nanosize anatase titania by aqueous sol–gel method

Titanylsulfate was used as the precursor for the preparation of nano titanium oxide. In a typical experiment, about 0.082 moles of titanylsulfate was dissolved in 500 mL distilled water and was hydrolyzed by adding ammonium hydroxide solution (25%) under constant stirring, until the pH of the precipitate was 7.5. The precipitate obtained was separated by filtration, washed free of sulfate ions (as confirmed by the $BaCl_2$ test) with distilled water and peptized by addition of 2 M HNO_3 solution until pH 1.8–2 to get the stable titania sol.

2.3. Synthesis of lanthanum phosphate sol

Lanthanum phosphate (20 g) was prepared by reacting lanthanum nitrate (0.0855 moles) with orthophosphoric acid (0.0855 moles) under constant stirring. The precipitate formed was flocculated by slow addition of 25% ammonia solution under constant stirring until pH 6. The filtrate was then washed with hot water, to remove the nitrates and excess phosphates. The washings were analyzed for phosphorus with ammonium molybdate and oxalic acid. The precipitate was then peptized in distilled water by adding 20% nitric acid and maintaining the pH between 1.8 and 2.2. The suspension was kept under stirring for about 4 h, when a stable sol was obtained.

2.4. Preparation of TiO_2–$LaPO_4$ nanocomposite sols

In order to obtain the nanocomposite sol of TiO_2 and lanthanum phosphate, calculated volumes of $LaPO_4$ (0.5 M) were added drop wise to the TiO_2 sol under constant stirring. A stable sol was obtained after 3 h stirring. The lanthanum phosphate concentration was varied from 0 to 50 mol% in the TiO_2–$LaPO_4$ composites and such materials are referred to as TLx, where x is the $LaPO_4$ content (0–50 mol%). Prepared sols were dried and annealed at varying temperatures (400, 600, 700, 800 and 900 °C) with 1 °C min^{-1} ramp and 3 h exposure time. The calcined powders were characterized by various techniques.

2.5. Coating experiments

Titania sols with an average particle size of ~50 nm and $LaPO_4$ sols with ~75 nm average particles were used to prepare suspensions for coatings on glass surfaces. Both TiO_2 and $LaPO_4$ sols had a solid loading of ~10 g L^{-1}. Optical glass slides (length 50 mm, breadth 24 mm and thickness ~1 mm) were surface treated with ~12 M nitric acid followed by washing with distilled water. Glass slides were coated with different sols at 25 °C using a dip coater unit supplied by KSV Instruments with an advancing and receding rate of 20 mm min^{-1} and holding for a minute. The coated glass slides were dried at 70 °C for 5 h and then annealed at 400 °C for 3 h and tested for water contact angles.

2.6. Characterization

X-ray diffraction (XRD) patterns of calcined powders were taken in X'pert PRO, Philips, diffractometer, in the 2θ range 20–60° using Cu$K\alpha$ radiation at a scan rate of 2 min^{-1} and a step size of 0.021°. The crystallite size was calculated using the Scherrer formula [19] as given in

$$D_{XRD} = \frac{k\lambda}{\beta \cos\theta} \quad (1)$$

where D_{XRD} is the average crystallite size, k, the shape factor (=0.9), λ the X-ray wavelength (Cu$K\alpha$, 1.5406 Å), β is the full width at half maximum of (101) peak of anatase and θ is the Bragg angle. The amount of rutile in the calcined samples was estimated using the Spurr equation [20]:

$$F_R = \frac{1}{[1+\{0.8 I_A(101)/I_R(110)\}]} \quad (2)$$

where F_R is the mass fraction of rutile in the sample and I_A (101) and I_R (110) are the integrated main peak intensities of anatase and rutile, respectively. Fourier transform infrared (FTIR) spectra were recorded in a Magna 560, Nicolet, Madison, Wisconsin spectrophotometer in the 4000–400 cm^{-1} range on powder samples dispersed in KBr pellets. The crystal structure and particle size of calcined titania powders were determined from high-resolution transmission electron microscopy data using a FEI Tecnai 30 G^2 S-Twin HR-TEM equipped with a Gatan CCD camera and operated at 300 kV. Brunauer, Emmett and Teller (BET) surface area measurements were carried out by nitrogen adsorption at 77 K using a Micromeritics Gemini 2375 surface area analyzer after degassing the samples at 200 °C for 2 h. Average pore diameters were derived from the N_2 adsorption–desorption

isotherms by the BJH method. The transmittance spectra of the coated and uncoated glass slides were recorded by a Shimadzu UV-2401PC Spectrophotometer in the spectral range 200–800 nm. Atomic force microscopy (AFM) images were recorded under ambient conditions using a NTEGRA (NT-MDT) operating with a tapping mode regime. Micro-fabricated TiN cantilever tips (NSG10) with a resonance frequency of 299 kHz and a spring constant of 20–80 N m^{-1} were used.

2.7. Measurement of photocatalytic activity

The photocatalytic activity of calcined powders was studied by monitoring the degradation of MB dye under UV exposure in an aqueous suspension of TiO_2 or TiO_2–$LaPO_4$ nanocomposite under constant magnetic stirring. Approximately 0.1 g of powdered TiO_2, dispersed in 100 mL water was mixed with an aqueous solution of MB (1.25×10^{-5} M). The suspension was stirred in the dark for 30 min to allow for full adsorption of MB dye by the nanocrystalline TiO_2 powders. The suspension was then exposed to UV light in a Rayonet photoreactor under constant stirring. The UV source was twenty four 15 W tubes (Philips G15T8) emitting UV radiation in the region 200–400 nm with an intensity of 10 mW cm^{-2}. After each exposure, ~5 mL of suspension was taken out from the irradiation chamber at intervals of 20, 40, 60, 80, 100 and 120 min. The powder was separated out of the suspension using a table top centrifuge at 3000*g* rcf. The filtrate was then examined using a UV–visible spectrometer (UV-2401PC, Shimadzu, Japan), to study the degradation of the aqueous MB solution in visible light. The absorption spectra of the MB dye solution were obtained in the range of 200–800 nm and as a function of exposure time. The absorption maximum at 656 nm in the spectrum of MB was used to determine the concentration. The initial absorbance (A_0) was obtained from the UV–vis spectrum of the MB suspension, stirred in the dark and without the UV light exposure and was taken as the initial MB dye concentration (C_0). The absorbance (A) of MB solutions, after irradiation time intervals of 20, 40, 60, 80, 100 and 120 min, was taken as a measure of the residual concentration, C, of the MB dye. The efficiency of degradation was calculated from a formula as follows:

$$\frac{C}{C_0} = \frac{A_{t=t}}{A_{t=0}} \tag{3}$$

where $A_{t=0}$ is the initial absorbance of MB solution and $A_{t=t}$ is the absorbance values after the fixed time intervals. The photocatalytic decomposition of the organic molecules follows the Langmuir–Hinshelwood kinetics [21], which may be represented as

$$\frac{dC}{dt} = k_{app}C \tag{4}$$

where 'dC/dt' represents the rate of change in the MB dye concentration with respect to the irradiation time 't', 'k_{app}' the apparent first-order reaction rate constant and 'C' the concentration of the MB dye. Ln C_0/C was plotted against different times of UV exposure. The rate of degradation, k_{app}, was obtained from the slope of the linear regression of ln C_0/C versus exposure time plot. A control experiment was performed with MB dye solution in the absence of photocatalyst powder under continuous UV exposure. The initial MB dye concentration remained unchanged even after irradiating the sample for total 2 h. Because of small dimensions of glass substrates and thin nature of the coating, the amount of TiO_2 catalyst available in every coated slide was too small to cause a detectable catalytic decomposition of MB dye in our experiment in a timescale of even 10 h. In the present study, the photoactivity experiments were carried out with coating precursor powder.

The static contact angle measurements on the coated slides were done by the sessile drop method in a Data Physics OCA 40 micro automatic contact angle meter. The contact angle was determined numerically by drawing a tangent at the contact point of the edge of the droplet with the glass slide. The dynamic water contact angle of the powder samples were measured using Data Physics DCAT 21 dynamic contact angle instrument and tensiometer.

3. Results and discussion

3.1. Structural characterization

The crystalline phase identification in both pure and TiO_2–$LaPO_4$ composite powders, calcined at 800 °C, as characterized by X-ray

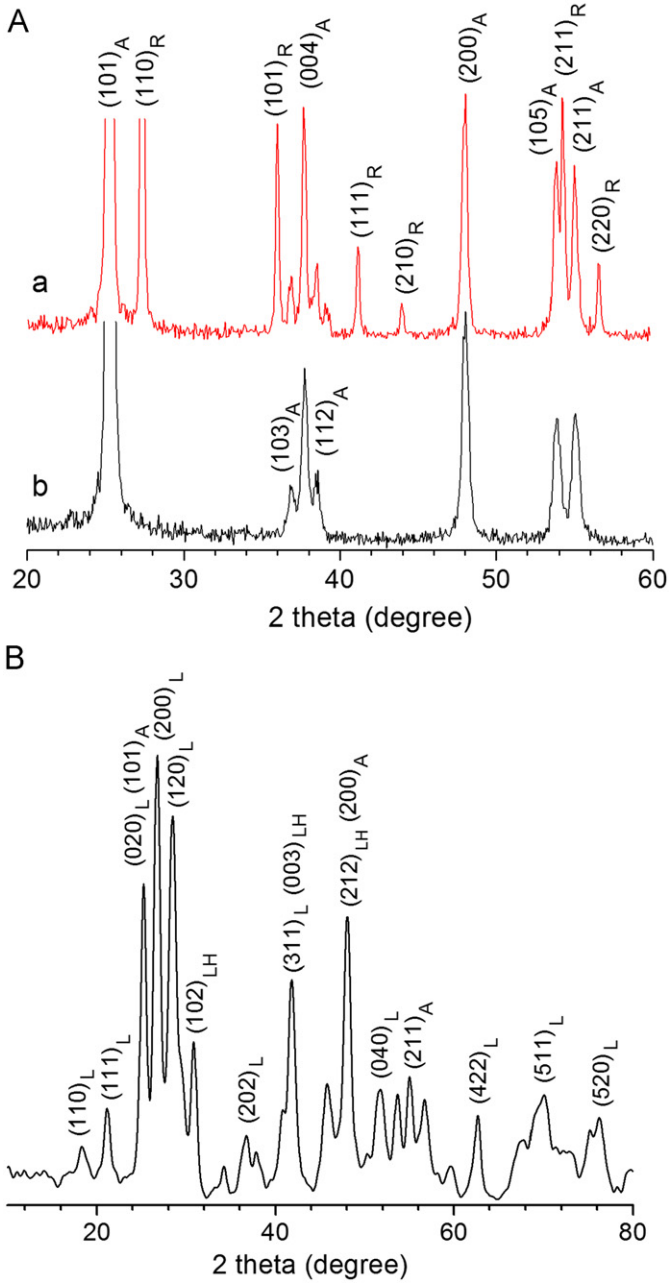

Fig. 1. (A) X-ray diffraction patterns of pure TiO_2 and TiO_2–$LaPO_4$ composite powders: (a) TL0 and (b) TL1, annealed at 800 °C. (B) X-ray diffraction pattern of TL50 composite powder, annealed at 800 °C. A, R, L and LH marked in the patterns represent anatase, rutile, $LaPO_4$ and $LaPO_4 \cdot 0.5H_2O$, respectively.

powder diffraction measurements is shown in Fig. 1. Most of the prominent diffraction peaks in the samples are indexed and marked. All the diffraction peaks seen in TL1 correspond to the anatase phase of TiO_2 (JCPDS card No. 21-1272) only, whereas, in the case of TL50, peaks characteristic to monazitic $LaPO_4$ (both anhydrous, JCPDS card No. 46-1326 and hydrous form, JCPDS card No. 46-1439) are also seen in addition to the peaks belonging to anatase phase. In $LaPO_4$ structure lanthanide atoms are coordinated by nine neighboring oxygen atoms, which form a polyhedron of pentagonal interpenetrating tetrahedral [22]. X-ray peaks attributed to rutile (JCPDS card No. 21-1276) and anatase forms were observed in pure TiO_2 (TL0) calcined at 800 °C. The anatase phase is fully stabilized even at 800 °C by the $LaPO_4$ addition. This is due to the decrease in number of intergranular contacts among titania grains by incorporation of $LaPO_4$, which leads to inhibition of grain growth by reducing the critical size for the formation of rutile nuclei [23–25].

The crystallite sizes of anatase crystals were determined from XRD using the Scherrer equation and are 24.4, 18.5 and 13.6 nm for TL0, TL1 and TL50, respectively. The average crystal diameter D_{XRD} of anatase shows a gradual decrease with the increase of $LaPO_4$ content due to the restriction of grain growth by the $LaPO_4$ barrier among the TiO_2 grains [23].

Fourier Transform Infrared spectra of the pure TiO_2 and TL1 calcined at 800 °C are presented in Fig. 2. A broad band centered around 3400 cm^{-1} indicates the presence of an –OH group (O–H stretching vibrations) on the surface of the powder at 800 °C, and the band around 1630 cm^{-1} indicates the presence of structural water (H–O–H bending vibrations) [26]. A small band centered around 1370 cm^{-1} is due to N–O stretching vibrations, indicating the presence of NO_3^- ions [27]. Peaks below 1000 cm^{-1} correspond to Ti–O and Ti–O–Ti bending vibrations [28].

The peak at 1040 cm^{-1} in TL50 is due to the phosphate P–O stretching and those around 615 and 540 cm^{-1} correspond to the O═P–O bending and O–P–O bending modes, respectively [17]. The peaks are identical for TL1 annealed at 400 and 800 °C.

The UV–vis transmittance spectra on coated glass substrates, annealed at 400 °C, have been carried out. The coatings with pure TiO_2 and TiO_2–$LaPO_4$ nanocomposite thin films have a transmittance between 91 and 98% within the visible region (400–800 nm). A decrease in transmittance is observed from 99% for uncoated glass slide to 91% for TiO_2 coated glass surface, annealed at 400 °C. TL1 is almost transparent with absorption of ~3.5% at a wavelength of 500 nm. A significant decrease in the transmittance below 400 nm can be attributed to absorption of light by anatase TiO_2 in the thin film. This leads to the excitation of electrons from the valence band to the conduction band of titania [29]. Lanthanum phosphate addition to TiO_2 shows higher transparency, 96.5% in TL1 and 98% in TL50, for the coated surfaces.

Specific surface area (BET), pore volume and pore diameter of different compositions, annealed at 400 and 800 °C, are presented in Table 1. BET surface area of TiO_2 was found to increase with increase in $LaPO_4$ content. By increasing the calcination temperature from 400 to 800 °C, BET surface area decreased in both the cases. An increase in the S_{BET} by the addition of $LaPO_4$ is due to the decrease in the crystallite size of anatase [11]. This is also an indication of restriction of grain growth by lanthanum phosphate among the grains. Particle coarsening at higher temperatures leads to decrease in pore volume by the collapse of the porous structure [30]. This is reflected in the total pore volume and the

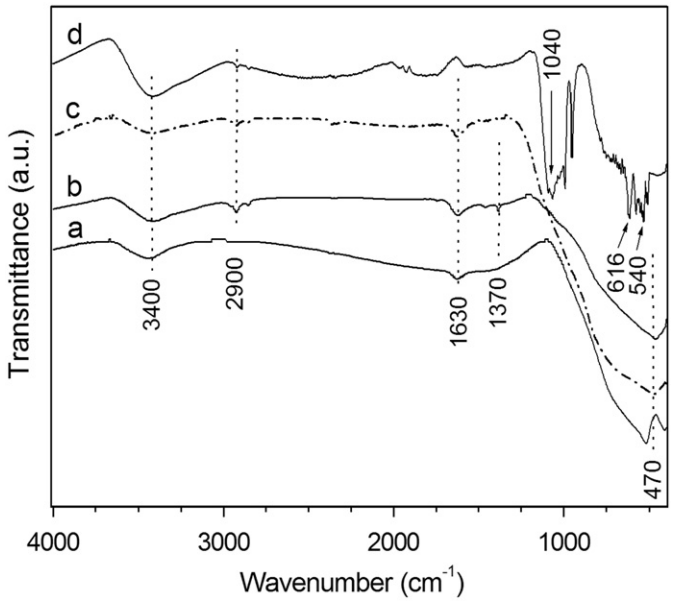

Fig. 2. Fourier transform infrared spectra of (a) TL0 annealed at 800 °C, (b) TL1 annealed at 400 °C, (c) TL1 annealed at 800 °C and (d) TL50 annealed at 800 °C.

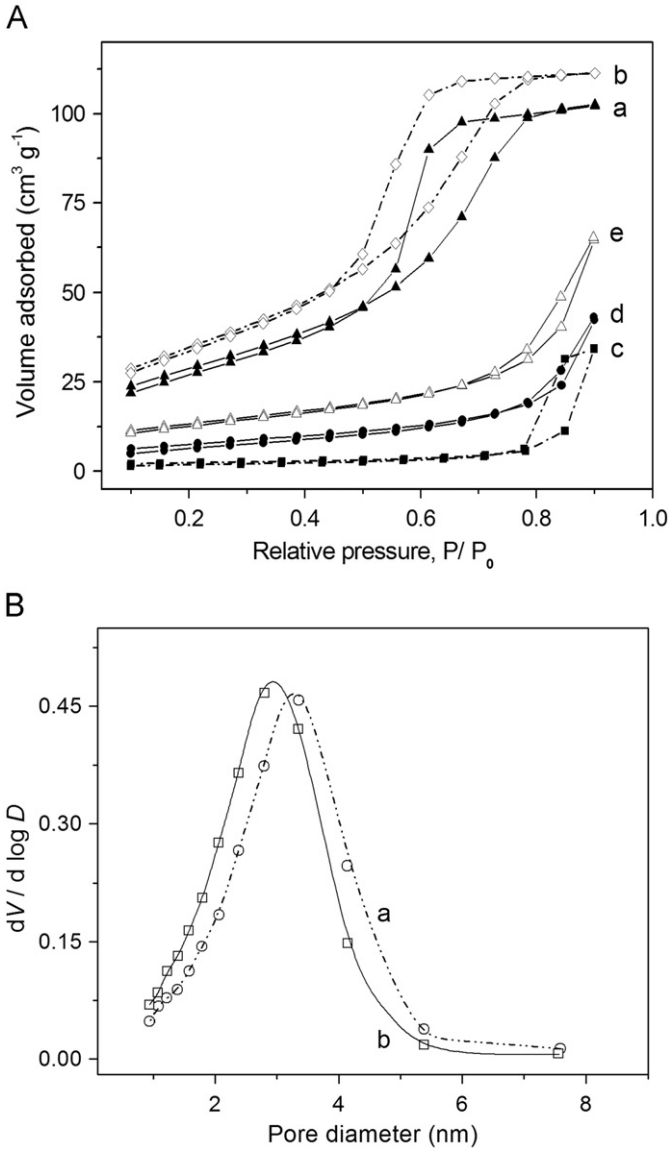

Fig. 3. (A) Adsorption–desorption isotherms of titania–lanthanum phosphate composite powders, calcined at different temperatures: (a) TL0 400, (b) TL1 400, (c) TL0 800, (d) TL1 800 and (e) TL50 800 °C. (B) pore size distribution curves of (a) TL0 and (b) TL1, calcined at 400 °C.

average pore diameter as seen in Table 1. While the pore volume marginally increased in the case of TL1 on heating at 400 °C, there is a substantial reduction on increasing the annealing temperature to 800 °C. The increase in specific surface area in the case of TL1 can be justified by the reduction in particle diameter (D_{TEM}) of TiO_2 from 26.8 nm in pure TiO_2 to 18.8 nm in TL1. Upon subsequent heating to 800 °C, the pore coarsening resulted in a considerable increase in pore diameter with a corresponding reduction in surface area [31]. Adsorption isotherms and pore size distribution of certain selected compositions, calcined at various temperatures, are presented in Fig. 3. All the isotherms exhibited typical type IV behavior with a hysteresis loop caused by capillary condensations within the mesopores. Both TL0 and TL1 show a monomodal distribution of pores in the meso range.

Table 1
Specific surface area, pore volume and pore diameter of TL0, TL1 and TL50, annealed at 400 and 800 °C.

Sample	Temperature (°C)	BET surface area ($m^2\,g^{-1}$)	Pore volume ($cm^3\,g^{-1}$)	Pore diameter (Å)
$LaPO_4$	400	102.0 ± 0.65		80.0
TL0	400	106.5 ± 0.35	0.1605	29.6
TL1	400	128.5 ± 0.41	0.1755	26.8
$LaPO_4$	800	54.0 ± 0.4		170.0
TL0	800	07.4 ± 0.17	0.0529	143.5
TL1	800	27.6 ± 0.11	0.0663	48.3
TL50	800	47.0 ± 0.38	0.0017	50.5

Average pore diameters obtained for TL0 and TL1 are 2.9 and 2.6 nm, respectively. Volume adsorption was higher for nanocomposites than pure TiO_2, which indicates a slightly higher surface area. High temperature calcination of titania powder resulted in a mesoporous solid with a wide pore size distribution and low porosity (Table 1).

The bright field HR-TEM images of TL0, TL1 and TL50, calcined at 800 °C, are presented in Fig. 4. The average size of particles from TEM (D_{TEM}) is calculated by measuring the sizes of over 100 particles from multiple TEM images. Sample TL0 consists of ~60% anatase crystals of size 26.8 nm and the rest are large rutile particles of ~95.7 nm size. However, by the addition of 1 mol% $LaPO_4$, TiO_2 nanocrystals (anatase) show sizes in the range 4.6–39 nm with a decrease in average size (D_{TEM}) to ~18.8 nm in TL1 (Fig. 4B). The composite powder TL50 (Fig. 4C and D) calcined at 800 °C consists of rod shaped particles of $LaPO_4$ of average diameter ~15 nm and length ~65 nm (ESD 28 nm) and spheroidal anatase particles of sizes in the range 3.6–35 nm with an average ~14.5 nm. The nine-coordinate lanthanide atoms combine apically with distorted tetrahedral PO_4^{3-} groups to form chains along the (0 0 1) direction, which induces the intrinsic anisotropic growth of $LaPO_4$ into nanorods [22]. Anatase crystal size (D_{XRD}) in TL1 is 18.5 nm and the same in TL50 is 13.6 nm and are very close to their respective sizes (D_{TEM}) obtained from TEM measurements (18.8 and 14.5 nm, respectively). Fig. 4D shows that $LaPO_4$ and TiO_2 components in the composite powder TL50 are highly crystalline as indicated by the presence of sharp crystal facets in the HR-TEM image.

Fig. 4D shows lattice fringes corresponding to (101), (200) and (004) planes of anatase with respective interplanar spacing

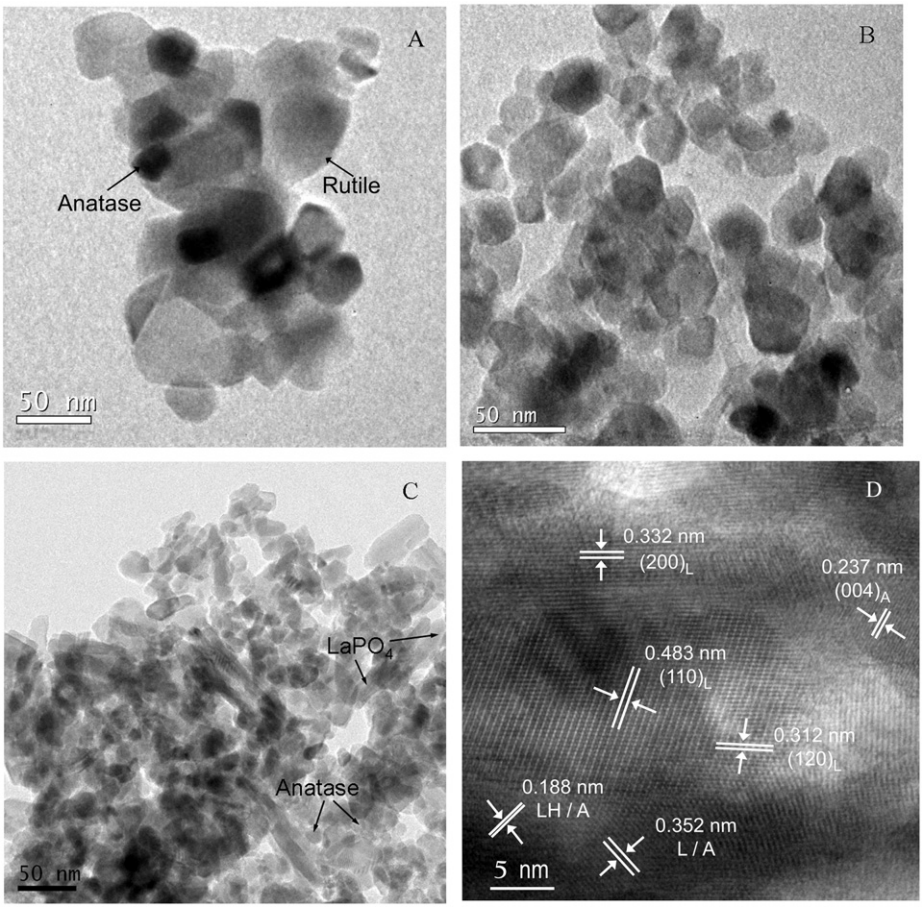

Fig. 4. Transmission electron microscopy (TEM) images of (A) TL0, (B) TL1, (C) TL50 and (D) HR-TEM image of TL50, all calcined at 800 °C.

of 0.352, 0.188 and 0.237 nm. Lanthanum phosphate phase is identified by the presence of crystal facets corresponding to (200), (120), (020) and (110) planes with interplanar spacing of 0.332, 0.312, 0.352 and 0.483 nm, respectively. The results are consistent with the XRD data (Fig. 1). The lattice fringes with *d*-spacing 0.188 nm are attributed to the (212) planes of hydrated lanthanum phosphate and (200) planes of anatase TiO_2.

3.2. Measurement of photocatalytic activity

The relative photocatalytic behavior of TL1, annealed at different temperatures in the range 400–900 °C, is presented as residual MB dye concentration against light exposure time in Fig. 5. The change in photocatalytic activity for powders as a function of annealing temperature is almost linear as indicated by the linear regression with fitting errors in the range 0.92–0.99. The MB dye degradation was the highest (95.1%) for the composite powder TL1, annealed at 800 °C on light exposure for 120 min, and was found to follow the order of annealing temperatures 800 > 700 > 600 > 400 °C.

The photodegradation of MB by nanosized TL1 increased with increasing the crystallinity (increase in crystal diameter) of the majority anatase phase. The crystal diameter (D_{XRD}) of anatase in TL1 increased from 9.8 to 18.5 nm on increasing the annealing temperature from 400 to 800 °C. As a result, the surface area is reduced considerably from ~128 to ~27 $m^2\,g^{-1}$ for TL1, upon increasing the annealing temperature from 400 to 800 °C. The increased crystallinity of anatase without the formation of rutile phase is desirable to achieve higher photoactivity [32]. The phase transformation of anatase to rutile was suppressed even at 800 °C by the presence of $LaPO_4$ in TL1 (Fig. 1).

The photocatalytic reaction can be summarized as follows:

$$TiO_2 + h\nu \rightarrow TiO_2 + h^+ + e^-$$

$$OH^- + h^+ \rightarrow OH^\bullet$$

$$O_2 + e^- \rightarrow O_2^-$$

MB degradation is mainly happening by the successive attacks of the formed OH radicals. The enhanced photocatalytic activity of TiO_2–$LaPO_4$ can also be explained as the effective interfaces exposed to the surface by the two components, where the photocatalytic reactions take place [12].

When the annealing temperature was raised to 900 °C, a decrease in the photocatalytic activity is observed in TL1 due to formation of ~53% rutile phase [33,34]. Typical variations in the remaining MB dye concentration as a function of UV exposure time and the calculated activity for the composite powders, annealed at 800 °C, are shown in Fig. 6. TL1 has the highest photocatalytic activity with apparent rate constant (k_{app}) $24 \times 10^{-3}\ min^{-1}$ with an optimum 1 mol% $LaPO_4$ in the composition. While 95.1% degradation was observed with TL1, only 70% degradation was observed in the case of pure TiO_2, annealed at 800 °C, after 120 min of light exposure ($k_{app} = 9.6 \times 10^{-3}\ min^{-1}$). The highest photoactivity (k_{app}) achieved with pure TiO_2 (TL0) is $\sim 18.5 \times 10^{-3}\ min^{-1}$ on annealing the catalyst at 700 °C.

The lower activity ($k_{app} = 7.8 \times 10^{-3}\ min^{-1}$) of TL0.5 can be attributed to the higher crystallite size of ~23.9 nm (not presented here) and low BET surface area (~18.0 $m^2\,g^{-1}$) [35]. The MB dye degradation was extremely small (9.5%) by the composite powder TL50 containing 50 mol% $LaPO_4$. This is attributed to inactive $LaPO_4$ crystals that partially cover the anatase particle

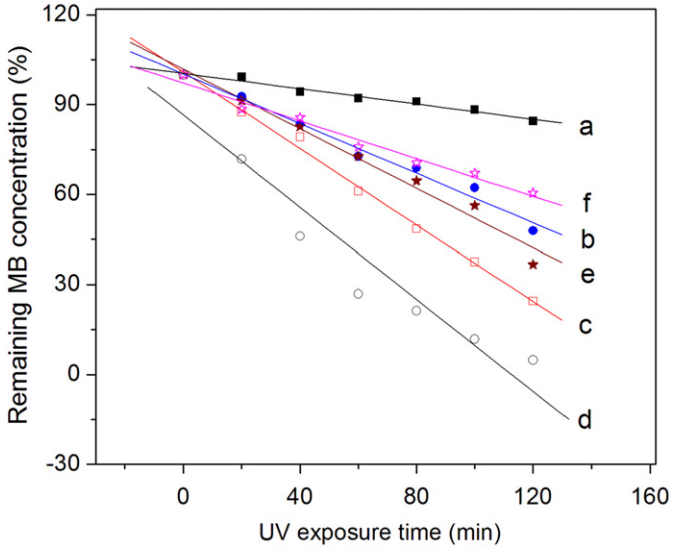

Fig. 5. Variation in the residual MB dye concentration as a function of UV exposure time with different time intervals for TL1 powders, annealed at (a) 400, (b) 600, (c) 700, (d) 800, (e) 900 °C and (f) Hombikat UV 100. The solid lines through the data points are the respective linear fits.

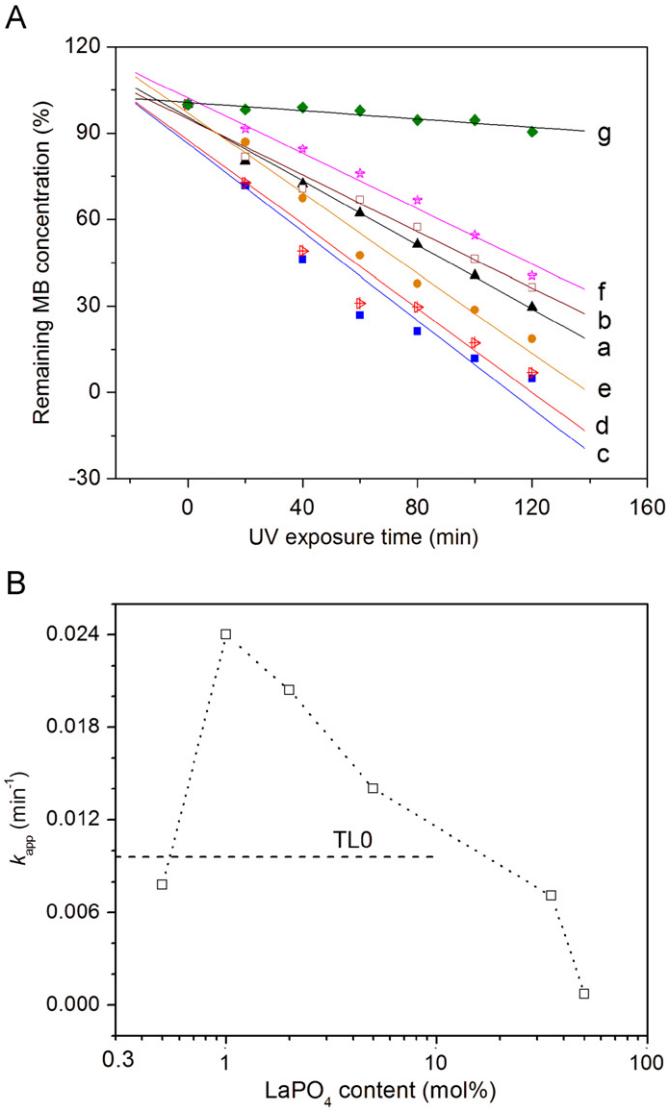

Fig. 6. (A) Variation in the residual MB dye concentration as a function of UV-exposure time for (a) TL0, (b) TL0.5, (c) TL1, (d) TL2, (e) TL5, (f) TL35 and (g) TL50. (B) Apparent first order rate constant, k_{app}, for the degradation of MB dye as a function of $LaPO_4$ content in TiO_2–$LaPO_4$ compositions, all calcined at 800 °C.

surfaces and absorb part of the radiation. The amount of TiO_2 available for the photocatalysis is less when the lanthanum phosphate concentration is increased to 50 mol% in the TiO_2 system. As a result, complete anatase population do not take part in the photocatalytic process, decreasing the activity of TL50 ($k_{app}=0.7\times10^{-3}$ min^{-1}).

The catalytic behavior in the photodegradation of MB compared with the data already reported in the literature is shown in Table 2, which clearly indicates that our data on photoactivity is comparable to those published in the literature.

Table 2
Comparison of photocatalytic activity of present work with some of the earlier reports.

Photocatalyst	Preparation method	Calcination temperature (°C)	Decolorization of dye (%) (time/h)
Degussa P25	Commercial	–	100 (6) [36]
ZnO/In_2O_3	Co-precipitation	800	93 (3) [12]
SnO_2/TiO_2 nanotubes	Solvothermal	–	95 (0.33)[37]
CNT/TiO_2	Refluxing	700	60 (1) [38]
Present work	Aqueous sol–gel	800	95 (2)

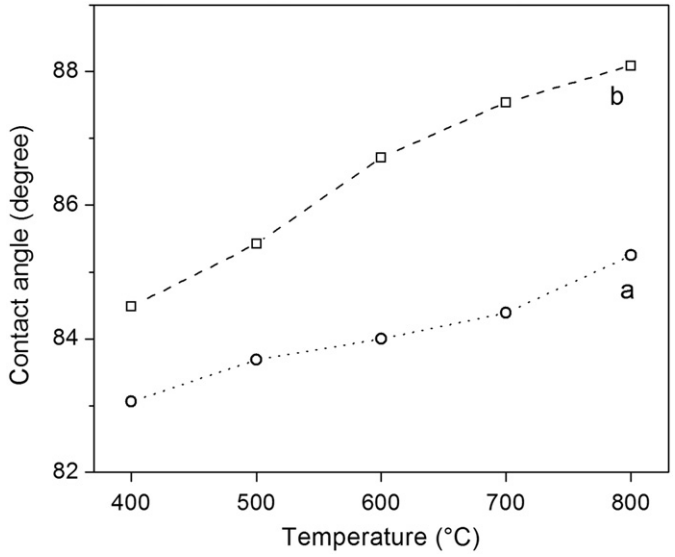

Fig. 7. Variation of contact angle values as a function of annealing temperature for the powders (a) TL1 and (b) TL50.

3.3. Measurement of hydrophobicity

The hydrophobicity of TiO_2–$LaPO_4$ nanocomposite powders has been studied by dynamic contact angle measurements. The variation in hydrophobicity of TL1 and TL50 powders, calcined at different temperatures, is shown in Fig. 7. The water contact angle values and hence, the hydrophobicity, of the powders increased with increase in annealing temperature in the order, 400 < 500 < 600 < 700 < 800 °C.

This may be due to the decrease in surface hydroxyl functionalities in powders annealed at higher temperatures [39]. The surface profile of glass slides, coated with TiO_2–$LaPO_4$ composites and annealed at 400 °C, using atomic force microscopy, is presented in Fig. 8. From the AFM micrograph, it is obvious that the peaks and valleys grew substantially on the coated surface with increase in $LaPO_4$ content in the TiO_2–$LaPO_4$ composite.

The average surface roughness (R_A) was 6.5, 13.5 and 39.2 nm for the surfaces coated with TL0, TL1 and TL50, respectively. The water contact angle data on the uncoated glass slide as well as glass surfaces coated with different TiO_2–$LaPO_4$ composites is presented in Fig. 9. Surface roughness is known to play an important role in hydrophobicity [2]. Hydrophobicity as measured by water contact angles on coated slide was found to increase with increase in the surface roughness (Fig. 9).

The contact angles for the different compositions of TiO_2–$LaPO_4$ coatings with 0, 0.5, 1, 35 and 50 mol% $LaPO_4$ are 62, 65, 73.9, 82.8 and 92.6, respectively, while for a pure $LaPO_4$ coating the contact angle is ~80° (not presented here). So an increase in hydrophobicity on the coated surface was observed with increase in $LaPO_4$ content in TiO_2–$LaPO_4$ composite, which had a concomitant increase in surface roughness.

Though a number of coating compositions (TiO_2–$LaPO_4$ with $LaPO_4$ > 1%), annealed at 400 °C, show better hydrophobicity, TL1

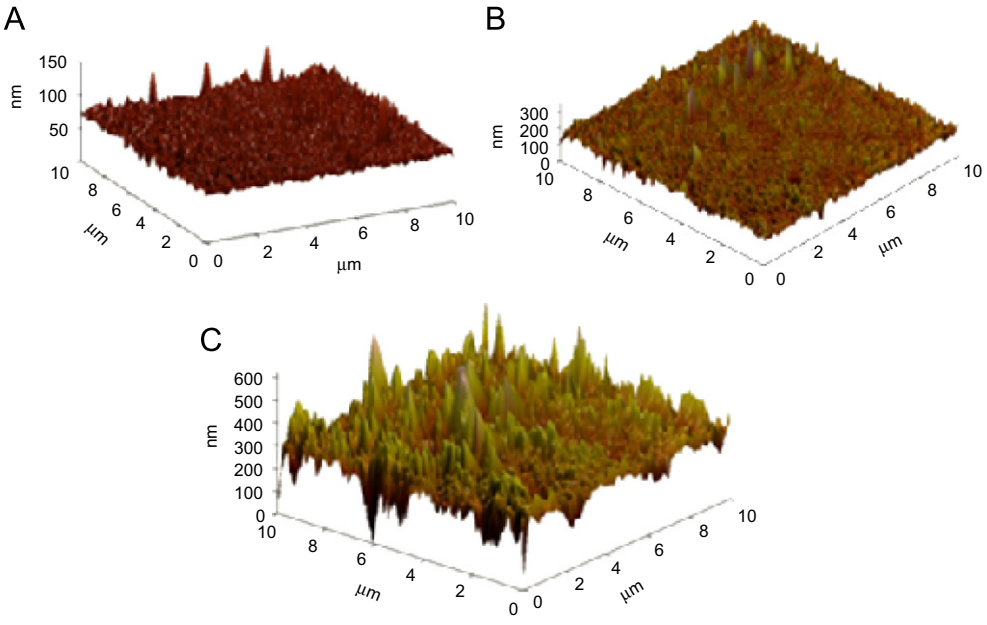

Fig. 8. The atomic force microscopy surface profiles of glass slides, coated with (A) TL0, (B) TL1 and (C) TL50, calcined at 400 °C.

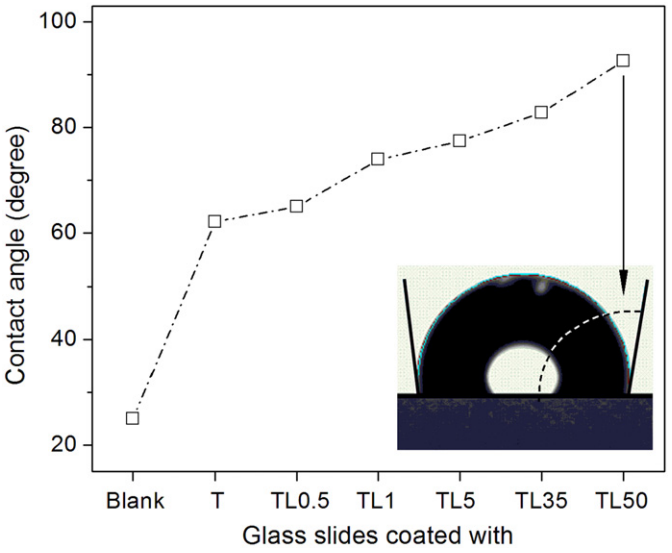

Fig. 9. Water contact angle measurements by sessile drop method on uncoated (blank) as well as TL0, TL0.5, TL1, TL5, TL35 and TL50 sol coated glass slides, annealed at 400 °C. Optical photograph depicting the resultant contact angle when a water drop is deposited on TL50 coated glass slide is shown in the inset.

has the moderate contact angle (73.9°). The TL1 powder, annealed at 800 °C, shows the highest photoactivity ($k_{app}=24\times10^{-3}$ min^{-1}) and powder contact angle ~85°. The above results suggest that TiO_2–$LaPO_4$ material is multifunctional and TL1 composition has the promise as an efficient self-cleaning precursor for both glass and tile surfaces.

4. Conclusions

Nano titanium dioxide and titania–lanthanum phosphate nanocomposites of different compositions have been synthesized by aqueous sol–gel processes and fully characterized by various techniques. Lanthanum phosphate has shown to be an excellent additive to titanium oxide for imparting increased anatase phase stability and enhanced hydrophobicity. Further, we could prepare almost transparent titania–lanthanum phosphate coating by dip coating. The present study has resulted in a novel approach to introduce hydrophobicity as well as photocatalytic activity to composite TiO_2–$LaPO_4$ coatings using inorganic precursors. Coating on a glass surface with the TL1 material has shown the optimum hydrophobicity and promising UV light photocatalytic activity, essential for achieving self-cleaning surfaces. Such hydrophobic and photoactive coating will reduce surface contamination on coated surfaces when exposed to the environment, such as large area solar panels in difficult to access locations, and similar exterior surfaces.

Acknowledgments

The authors are grateful to the Director, National Institute for Interdisciplinary Science & Technology (NIIST), CSIR, for providing the necessary facilities for the work. We thank Department of Science & Technology (DST) and CSIR, India, for providing HR-TEM facility to NIIST. MMD (X-ray), HR-TEM staffs are kindly acknowledged for their assistance in obtaining XRD and electron microscopy data. We thank staffs of Biomedical Wing, SCTIMST, Trivandrum, for providing contact angle measurements. The authors acknowledge the fruitful discussions with Dr. P. Shajesh. One of the authors (CKJ) acknowledges DST for the financial support. A special word of acknowledgement to Dr. Eoin Murray, IPRI, ARC (ACES), University of Wollongong, NSW, Australia, for technical discussions.

References

[1] X.T. Zhang, O. Sato, M. Taguchi, Y. Einaga, T. Murakami, A. Fujishima, Chem. Mater. 17 (2005) 696.
[2] X.M. Li, D. Reinhoudt, M. Crego-Calama, Chem. Soc. Rev. 36 (2007) 1350.
[3] W. Barthlott, C. Neinhuis, Planta 202 (1997) 1.
[4] R. Blossey, Nat. Mater. 2 (2003) 301.
[5] A. Scardino, R. De Nys, O. Ison, W. O'Connor, P. Steinberg, Biofouling 19 (2003) 221.
[6] H. Saito, K. Takai, H. Takazawa, G. Yamauchi, Mater. Sci. Res. Int. 3 (1997) 216.
[7] D. Quere, Rep. Prog. Phys. 68 (2005) 2495.
[8] M. Zielecka, E. Bujnowska, Prog. Org. Coat. 55 (2006) 160.
[9] A. Nakajima, K. Hashimoto, T. Watanabe, K. Takai, G. Yamauchi, A. Fujishima, Langmuir 16 (2000) 7044.
[10] M.K. Seery, R. George, P. Floris, S.C. Pillai, J. Photochem. Photobiol. A 189 (2007) 258.
[11] K. Rajesh, B. Sivakumar, P.K. Pillai, P. Mukundan, K.G.K. Warrier, V.R. Nair, Mater. Lett. 58 (2004) 1687.
[12] Z.Y. Wang, B.B. Huang, Y. Dai, X.Y. Qin, X.Y. Zhang, P. Wang, H.X. Liu, J.X. Yu, J. Phys. Chem. C 113 (2009) 4612.
[13] Y.Y. Liu, Z.Y. Wang, B.B. Huang, X.Y. Zhang, X.Y. Qin, Y. Dai, J. Colloid Interface Sci. 348 (2010) 211.
[14] S. Sasidharan, K.G.K. Warrier, J. Sol–Gel Sci. Technol. 58 (2011) 195.
[15] G.S. Devi, D. Giridhar, B.M. Reddy, J. Mol. Catal. A: Chem. 181 (2002) 173.
[16] Y. Takita, K. Sano, T. Muraya, H. Nishiguchi, N. Kawata, M. Ito, T. Akbay, T. Ishihara, Appl. Catal. A: Gen. 170 (1998) 23.
[17] K. Rajesh, P. Shajesh, O. Seidel, P. Mukundan, K.G.K. Warrier, Adv. Funct. Mater. 17 (2007) 1682.
[18] K. Ramesh, J. Zheng, E.G.Y. Ling, Y.F. Han, A. Borgna, J. Phys. Chem. C 113 (2009) 16530.
[19] S. Ghosh, D. Divya, K.C. Remani, T.S. Sreeremya, J. Nanopart. Res. 12 (2010) 1905.
[20] K.V. Baiju, P. Periyat, P. Shajesh, W. Wunderlich, K.A. Manjumol, V.S. Smitha, K.B. Jaimy, K.G.K. Warrier, J. Alloy. Compd. 505 (2010) 194.
[21] K.B. Jaimy, S. Ghosh, S. Sankar, K.G.K. Warrier, Mater. Res. Bull. 46 (2011) 914.
[22] Z.L. Chai, L. Gao, C. Wang, H.J. Zhang, R.K. Zheng, P.A. Webley, H.T. Wang, New J. Chem. 33 (2009) 1657.
[23] X.Z. Ding, X.H. Liu, J. Mater. Res. 13 (1998) 2556.
[24] K.N.P. Kumur, J. Engell, J. Kumar, K. Keizer, T. Okubo, M. Sadakata, J. Mater. Sci. Lett. 14 (1995) 1784.
[25] P. Nair, F. Mizukami, T. Okubo, J. Nair, K. Keizer, A.J. Burggraaf, AIChE J. 43 (1997) 2710.
[26] J.G. Yu, X.J. Zhao, Q.N. Zhao, Mater. Chem. Phys. 69 (2001) 25.
[27] S. Music, M. Gotic, M. Ivanda, S. Popovic, A. Turkovic, R. Trojko, A. Sekulic, K. Furic, Mat. Sci. Eng. B-Solid 47 (1997) 33.
[28] F. Cot, A. Larbot, G. Nabias, L. Cot, J. Eur. Ceram. Soc. 18 (1998) 2175.
[29] J.M.G. Amores, V.S. Escribano, M. Daturi, G. Busca, J. Mater. Sci. Lett. 6 (1996) 879.
[30] J. Zhu, J. Ren, Y.N. Huo, Z.F. Bian, H.X. Li, J. Phys. Chem. C 111 (2007) 18965.
[31] X. Chen, S.S. Mao, Chem. Rev. 107 (2007) 2891.
[32] K. Tanaka, M.F.V. Capule, T. Hisanaga, Chem. Phys. Lett. 187 (1991) 73.
[33] G. Liu, L.Z. Wang, H.G. Yang, H.M. Cheng, G.Q. Lu, J. Mater. Chem. 20 (2009) 831.
[34] C.P. Sibu, S.R. Kumar, P. Mukundan, K.G.K. Warrier, Chem. Mater. 14 (2002) 2876.
[35] V.S. Smitha, K.A. Manjumol, K.V. Baiju, S. Ghosh, P. Perumal, K.G.K. Warrier, J. Sol-Gel Sci. Technol. 54 (2010) 203.
[36] R.J. Tayade, T.S. Natarajan, H.C. Bajaj, Ind. Eng. Chem. Res. 48 (2009) 10262.
[37] L.R. Hou, C.Z. Yuan, Y. Peng, J. Hazard. Mater. 139 (2007) 310.
[38] M.L. Chen, F.J. Zhang, W.C. Oh, J. Korean Ceram. Soc. 45 (2008) 651.
[39] J.G. Yu, J.C. Yu, W.K. Ho, Z.T. Jiang, New J. Chem. 26 (2002) 607.